Macromolecular Symposia

www.ms-journal.de

Facile Synthesis and Morphology-Dependent Photocatalytic Activity of ZnO Nanostructures

Sapna Jadhav, Pradnya M. Bodhankar, Sameer Hadkar, Arwa Makki, Dina Hajjar, and Pradip B. Sarawade*

The structures of ZnO nanoparticles (NPs) of different morphology (rod, flower, and grains) using Zinc chloride and zinc nitrate synthesis are carried out under ambient conditions. In this investigation, we report that ZnO NPs are effectively synthesized and exploited to exhibit the morphological effect of ZnO NPS on its reduction in photocatalytic methylene blue (MB) dye-degradation. UV–Visible spectra studies of the prepared ZnO NPs confirm the absorption peak at 377, 376.3, and 376 nm representative of the formation of ZnO NPs. Powder X-ray diffraction (XRD) results demonstrate that the strong, highly intense, and narrow-width diffraction peaks indicate the most stable crystalline hexagonal (Wurtzite) structure of ZnO NPs of rod, flower, and grains with average size about 20, 16.62, and 18.02 nm in diameter, respectively. According to field emission-scanning electron microscopy (FE-SEM), results confirm the development of ZnO NPs. In addition, the degradation efficiency of MB dye by ZnO (grain) reveals larger enhancement than the rod and flower with the highest adsorption of color after 0.067 min^{-1}.This study offers the mainstep forward in the field of diluted wastewaters in textile industries.

1. Introduction

For several years, the environmental issue related to the decomposing hazardous pollutants has been the main engrossing attention of the world. Zinc oxide (ZnO) is described as one of the most significant and highly potential photocatalytic semiconductor substances due to its important physicochemical performance. ZnO nanostructures have enormous curiosity due to their features such as high electron mobility, wide-band gap, and great transparency in visible range.[1] The ZnO is an n-type semiconductor nanostructure that gained more attention due to satisfactory band gap (3.37 eV) and high binding energy (60 meV) NPs demonstrated around related band gaps.[2] The large excitation binding energy denotes the excessive emission in ZnO can maintain constant at room temperature and prominent.[3]

Morphology is one of the fundamental properties of catalysts in photocatalytic activity. For example, rod-shaped particles exhibit 5 times better performance than the hexagonal plate-shaped NPs for the degradation of methylene orange.[4] The catalytic function of nanostructures depends on the morphologies that influence the composition and a surface atomic arrangement,[5] which shows that the morphology of ZnO NPs can play a vital role in this research work. Presently, intensive research approaches are towards the controlling Physico-chemical properties of synthesized ZnO NPs with different precursors. The above results motivated the preference of ZnO material to study the effect of morphology on photocatalytic activity.

In the current research work, the synthesis of ZnO NPs with different precursors was reported. The morphology and structure of ZnO NPs were exploited to investigate the effect of morphology on the photocatalytic degradation process for the MB dye in aqueous heterogeneous suspension.

2. Experimental Section

2.1 Materials

The chemicals Zinc chloride ($ZnCl_2$), Zinc Nitrate $Zn(NO_3)_2 .6H_2O$, Ammonium fluoride (NH_4F), Ethanol, Sodium hydroxide (NaOH) were used in the synthesis of ZnO NPs. All reagent chemicals were obtained from Sigma Aldrich and utilized with no further purification. Double distilled water was utilized for preparing all aqueous solutions and washing purposes.

S. Jadhav
SDSMCollege
University of Mumbai
Palghar 401404, India
E-mail: jadhav.sapna@yahoo.com

S. Jadhav, P. M. Bodhankar, S. Hadkar, P. B. Sarawade
Departmentof Physics
University of Mumbai, Vidyanagari
Santacruz, Mumbai 400098, India

P. M. Bodhankar
National Centrefor Nanosciences and Nanotechnology
University of Mumbai, Vidyanagari
Santacruz, Mumbai 400098, India

A. Makki, D. Hajjar
Universityof Jeddah
College of Science
Department of Biochemistry
Jeddah 80327, KSA

The ORCID identification number(s) for the author(s) of this article can be found under https://doi.org/10.1002/masy.202100142

DOI: 10.1002/masy.202100142

2.2 Experimental Techniques

The in-depth synthesis process of ZnO NPs was as given below: The rod shape ZnO NPs were prepared using precursors of $ZnCl_2$. Initially, $ZnCl_2$ solution was prepared with 5.5 g of $ZnCl_2$ mixed in 100 mL of double distilled water under constant stirring up to the temperature reached 80°C. Then, the diluted NaOH solution was added dropwise to the $ZnCl_2$ solution under constant stirring at 80°C. The final solution turns milky, which indicates the formation of ZnO particles. The precipitate formed centrifuged and washed four times with ethanol subsequently with distilled water. The precipitate was dried for 12 h at 80°C in an oven. Finally, the ZnO NPs were obtained after calcination in a furnace under an air atmosphere at 400°C for 4 h. Another sample of ZnO NPs of flower and grain shape obtained with the precursor Zn $(NO_3)_2.6H_2O$. The ratio of Zn $(NO_3)_2.6H_2O$: NH_4F: NaOH::7.473:5.567: 8.004 and7.459: 1.850: 8.007 to retrieve flower and grain-shaped ZnO NPs, respectively. The same process followed to obtain flower and grain-shaped ZnO NPs.

2.3 Characterization of ZnO NPs

The synthesized nanostructured rod, flower, and grain-shaped ZnO NPs were characterized by physicochemical properties with X-ray diffraction (XRD), UV–visible spectroscopy, field emission scanning electron microscopy (FESEM), and Fourier transform infrared (FTIR) studies confirmed using Perkin Elmer (Model number 760, 400—4000 cm^{-1}) spectroscopy techniques. The XRD patterns were obtained with Cu Kα radiation (K = 1.54 Å) in the 2θ scan range of 10°–80°, and at the step interval of 0.02° with the counting time of 5 s at each point. The thermal stability of ZnO NPs was investigated by using a differential scanning calorimetry (DSC) instrument (SDT Q600). The characteristics of different morphology ZnO catalyst are summarized in **Table 1**.

Table 1. UV-vis peak, energy band gap, DSC peak, and grain size values of different morphology ZnO catalyst.

Catalysts	Absorbance [nm]	Energy band-gap [eV]	Grain size [nm]
ZnO(rod)	377	2.2	20
ZnO(flower)	376.3	2.06	16.62
ZnO(grain)	376	2.33	18.02

3. Results and Discussion

3.1. Morphological and Microstructural Analysis

The surface morphology of prepared ZnO NPs samples are recorded with FE-SEM.The stunning images of a rod **Figure 1**a,b, flower Figure 1c,d, and grain Figure 1e,f shaped ZnO NPs obtained from the reaction of different precursors with various solvents. The FESEM images demonstrated the set of different orientations with even morphology for ZnO powder.

3.2. Powder X-ray Diffraction (XRD) Analysis

The crystalline nature is studied by using Cu-Kα radiation (1.5406 A°) shown in the XRD profile. **Figure 2**a,b,c illustrates the XRD spectra of the obtained nanorod, flower, and grain-shaped ZnO NPs in the range of 2θ from 10° to 80°, respectively. The external form of the well-defined peaks at 2θ = 31.8°, 34.47°, 36.29°, 47.56°, 56.59°, 63.01°, 67.94°, and 69.07° are recognized to the planes with Miller-Bravais lattice indices of (100), (002), (101), (102), (110), (103), (112), and (201), respectively. The entire diffraction peaks confirming high-level purity of the powder of NPs fulfill with the JCPDS, card No. 01.080.0075 pattern of ZnO NPs demonstrate the hexagonal wurtzite crystalline nature.[6,7]

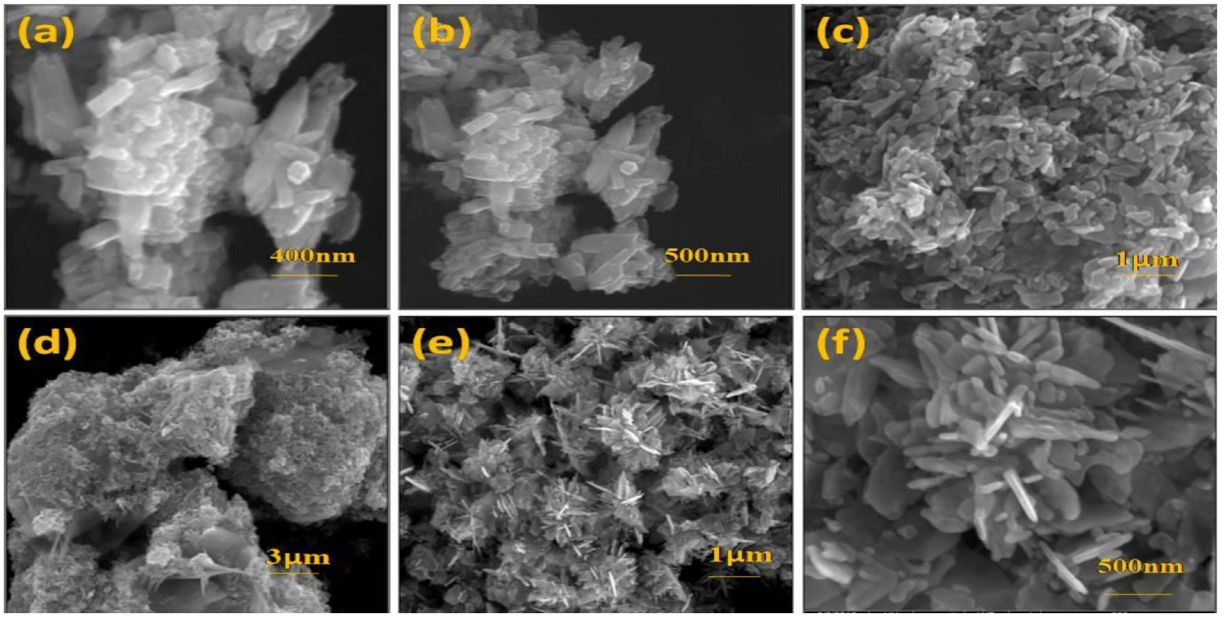

Figure 1. FESEM micrographs of ZnO: rod a) and b), flower c) and d), and grain e) and f) NPs.

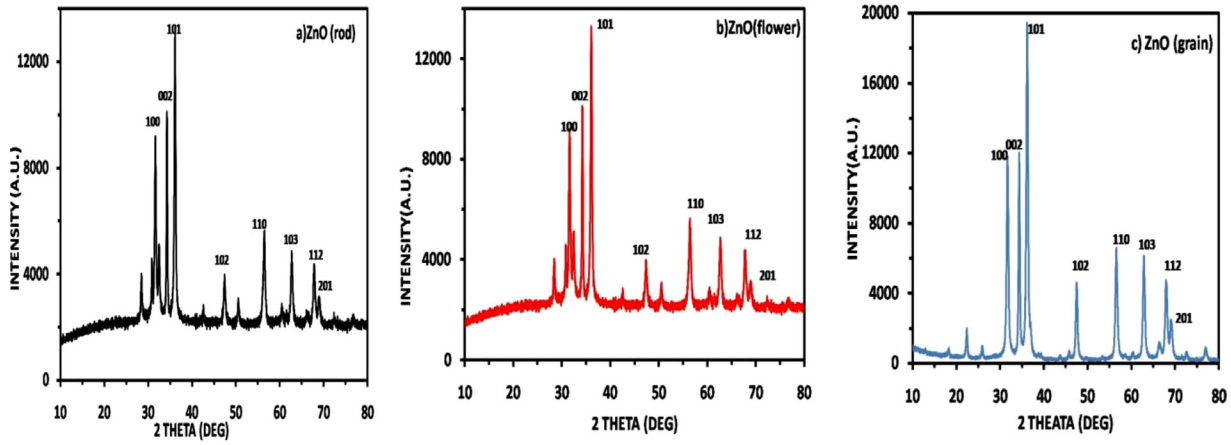

Figure 2. XRD spectrum of ZnO a) rod, b) flower, and c) grain NPs.

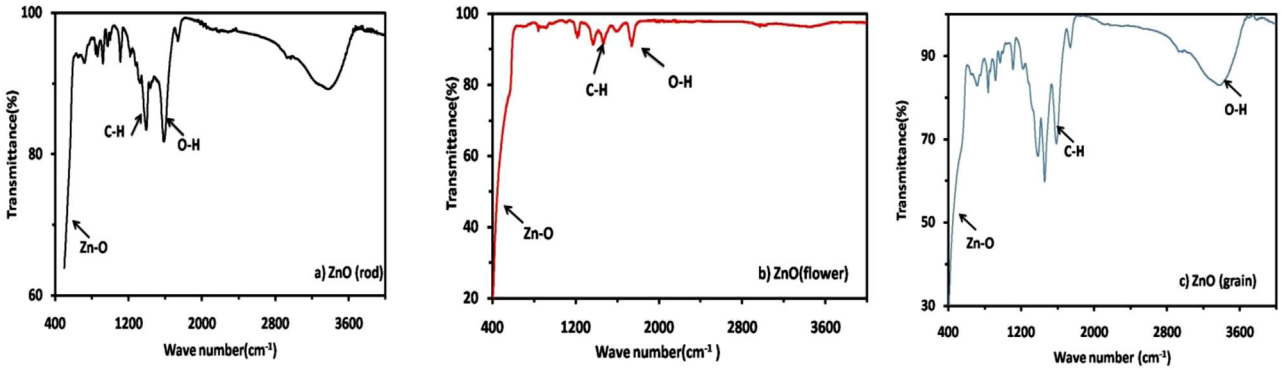

Figure 3. FTIR spectrum of ZnO a) rod, b) flower, and c) grain NPs.

The crystallite size "D" for ZnO NPs was predictable from the XRD crest measurement with the Debye-Scherer equation.[8]

$$D = 0.9\lambda/\beta\cos\theta \quad (1)$$

Where, λ is the wavelength (Cu-Kα), β is the full distance across at the half highest of the ZnO stroke and θ mentioned for the diffraction angle. The mean crystalline sizes measured by using the Debye-Scherer equation of ZnO nanostructures in nanorod, flower, and grain size were found to be 20, 16.62, 18.02 nm, respectively.

3.3. FTIR Study

As depicted in **Figure 3**, FTIR spectra of the prepared ZnO NPs implanted in the KBr matrix have been reported in the IR range (4000-400 cm^{-1}).Figure 3a,b,c illustrates the strong absorption peaks at 3375.66, 1738.71, 1587.51, 1457.63, 1385.04, 1110.38, and 839.01 cm^{-1} of different stretching modes in the IR spectra. The band near 1457.63 cm^{-1}indicates the H-O-H bending vibration mode of water molecules due to the moisture are absorbed by the ZnO powder. The absorption peak at 1385.04 cm^{-1} is due to the C-H bond.[9]

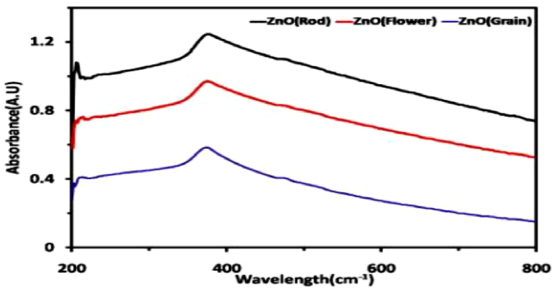

Figure 4. UV-Vis absorption spectra of ZnO a) rod, b) flower, and c) grain NPs.

3.4. UV-visible Spectral Study

Figure 4a,b,c illustrates the UV-Vis absorption spectrum of ZnO nanorod, flower, and grain. Strong absorption peaks are observed at ~377, 376.3, and 376 nm for nanorod, flower, and grain structures, respectively. These absorption peaks are blue-shifted with diminishing in the aspect of the nanomaterial and compared with the intensity of the ZnO sample normally of 373 nm certifying the quantum confinement. The bandgap energy is calculated by using the Planck-Einstein equation, $E = hc/\upsilon$, where, the Planck constant = h (6.63×10^{-34} J.s), the velocity of light = c (2.99×10^8 m s^{-1}) and the υ is the obtained absorption maxima (nm). The

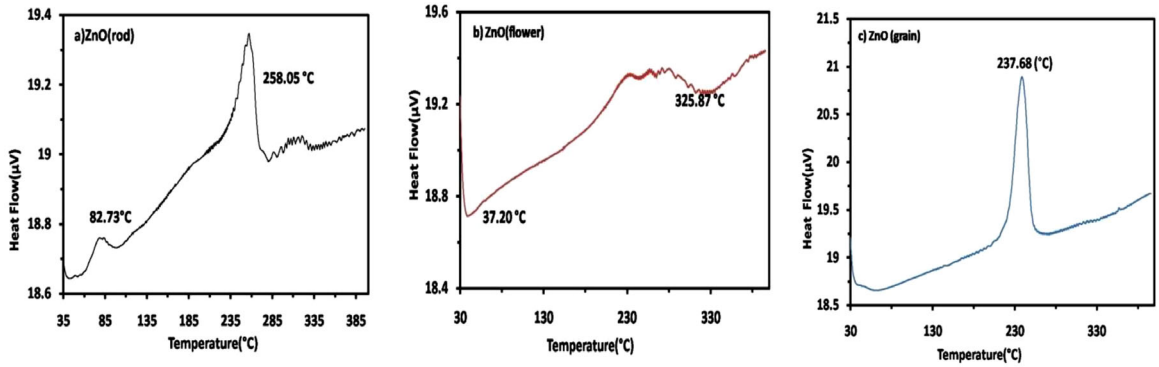

Figure 5. DSC plots of ZnO a) rod, b) flower, and c) grain NPs.

rise in the direct bandgap of the synthesized samples of nanorod, flower, and grain obtained as 2.20, 2.06, and 2.33 eV, respectively.

3.5. Differential Scanning Calorimeter (DSC) Analysis

To explore the effect of morphology on thermal properties of ZnO nanostructures, differential scanning calorimetric (DSC) analysis is investigated. **Figure 5**a,b,c depicts the domino effect of DSC analysis on ZnO nanostructure calculated at the constant heating rate of 10°C min^{-1} in the inert air. In conclusion, with an exothermic peak at 82.73°C and 258.05°C(rod), 237.68°C(grain) along with an endothermic peak at 37.20°C and 325.87°C (flower) is owing to result for melting or thermal degradation.

3.6. Photocatalytic Degradation Studies

3.6.1. Experimental Analysis

Methylene blue (MB) dye is a poisonous compound utilized for fabrics and wood dyeing purposes with the molecular formula $C_{16}H_{18}N_3SCl$. Initially, 30 mg of each ZnO catalyst material was dispersed in 50 mL of 10 mg aqueous MB solution. The photocatalytic reaction was performed under constant magnetic stirring at room temperature for uniform dispersion of the particles during a photocatalytic reaction. The UV-Vis spectral analysis of aqueous MB solution and ZnO irradiation to UV light was recorded every 15 min of irradiation.

3.6.2. Degradation Kinetics of Methylene Blue Solution

The UV–Vis spectra of MB solution irradiated to UV light. **Figure 6**a,b,c indicates the results of 0 min (dark) to the 120 min time interval were captured with UV–Visible instrument of a rod, flower, and grain NPs size catalyst. The steady reduction in the crest value of absorbance at dissimilar irradiation time is seen in Figure 6d experiment performed in the absence of ZnO under irradiation indicates that the blue color reduces at a slow pace. The degradation of blue color on the photocatalyst surface is a vital footstep in a photocatalytic degradation method. The color dye with excessive absorption decays quicker and

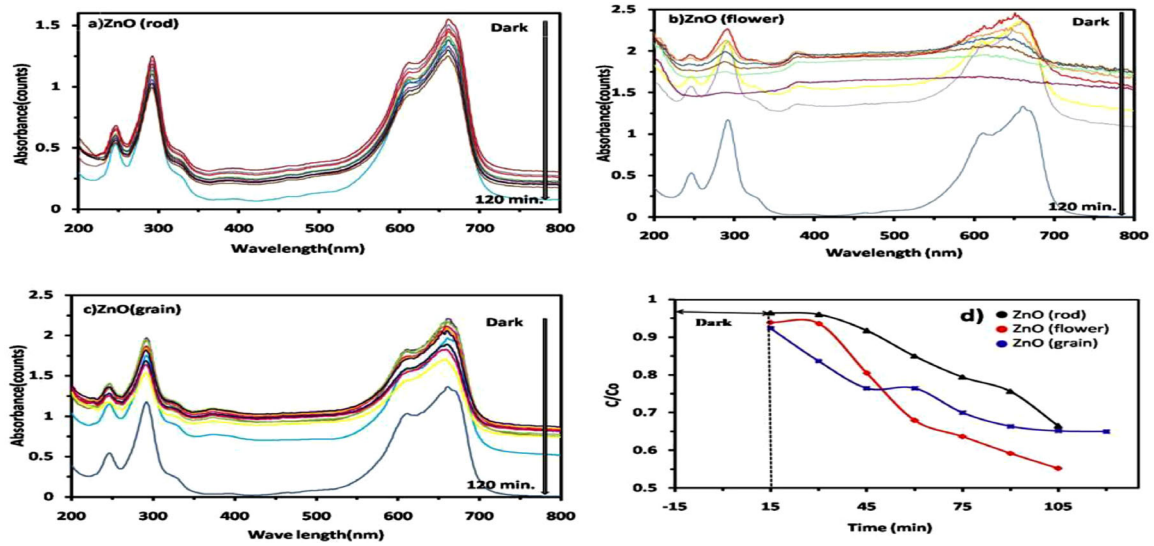

Figure 6. UV-Vis absorption spectra of Photocatalytic activity of a) rod, b) flower, and c) grain NPs for the decolorization of MB dye under UV-light irradiation. d) C/Co versus irradiation time for rod, flower, and grain nanostructures of ZnO.

hence the active sites of catalyst in effect absorb the UV light diminishes with increase in the impregnation of the dye color. The consulate effects are discovered in the graph of C/Co against time, shown in Figure 6d, where Co is the preliminary blue color of dye concentration and C is the dye concentration of the blue color after radiation for the time slot "t" in min. As per the consequences, the photocatalytic activity of ZnO (grain) shows better performance as compared to the rod and flower with the highest adsorption of color after 0.067 min^{-1}.

4. Conclusions

The integration of ZnO nanostructures with different morphology is a significant factor in mounting their application as photocatalytic degradation of MBdye. In this research, SEM analysis demonstrates the rod, flower, and grain morphology of the prepared ZnO nanostructures. The hexagonal wurtzite nanostructure of the crystalline nature of the synthesized nanostructures is certified from the XRD analysis. The size of nanorod, flower and grain NPs are 20, 16.62, and 18.02 nm, respectively, which shows dependent discrepancies of absorption is evaluated through UV-Vis absorption spectra. The exothermic and endothermic peaks indicate the melting or thermal degradation of the ZnO nanostructure. ZnO grains exhibit superior photocatalytic activity on the MB dye. By increasing irradiation time ZnO NPs, the precision of the samples decreased. The increase in adsorption rate and the slow down the recombination within electrons/holes pairs in ZnO grains to build them as useful morphology for better-quality photocatalytic than the rod and flower shape.

Acknowledgements

Pradip Sarawade acknowledges the University of Mumbai under minor research project, Department of Physics, University of Mumbai, and SERB grants (EEQ/2020/0002980) under DST for their financial support.

Conflict of Interest

The authors declare no conflict of interest.

Data Availability Statement

The data that support the findings of this study are available on request from the corresponding author. The data are not publicly available due to privacy or ethical restrictions.

Keywords

Keywords, industrial pollutants, methylene blue (MB), morphology, photocatalytic degradation, UV–Visible spectra

Received: April 16, 2021
Revised: May 28, 2021

[1] D. M. Fernandes, R. Silvaa, A. A. WinklerHechenleitner, E. Radovanovic, M. A. Custódio Melo, E. A. Gomez Pineda, *Mater. Chem. Phys.* **2009**, *115*, 110.
[2] S.-K. Kim, *Handbook of Marine Microalgae: Biotechnology Advances*, Academic Press, **2015**.
[3] S. A. Dahoumane, M. Mechouet, K. Wijesekera, C. D. Filipe, C. Sicard, D. A. Bazylinski, C. Jeffryes, *Green Chem.* **2017**, *19*, 552.
[4] A. McLaren, T. Valdes-Solis, G. Li, S. C. Tsang, *J. Am. Chem. Soc.* **2009**, *131*, 12540.
[5] Y. Lin, H. Hu, Y. H. Hu, *Applied Surface Sci* **2020**, *502*, 144202.
[6] F. Buazara, M. Bavi, F. Kroushawi, M. Halvani, A. Khaledi-Nasabe, S. A. Hossieni, *J. Exp. Nanosci.* **2016**, *11*, 175.
[7] G. Zhang, X. Shenand, Y. Yang, *J. Phys. Chem. C* **2011**, *115*, 7145.
[8] H. Friedman, L. S. Birks, *J. Appl. Phys.* **2004**, *17*, 687.
[9] E. Rusu, T. Gutul, N. Condur, V. Ursaki, E. Goncearenco, P. Vlazan, *Beilstein J. Nanotechnol.* **2014**, *5*, 402.